PHYSICAL REVIEW C **89**, 064305 (2014)

Transition from collectivity to single-particle degrees of freedom from magnetic moment measurements on ${}^{82}_{38}\mathrm{Sr}_{44}$ and ${}^{90}_{38}\mathrm{Sr}_{52}$

G. J. Kumbartzki,* N. Benczer-Koller, S. Burcher, A. Ratkiewicz, S. L. Rice, Y. Y. Sharon, and L. Zamick
Department of Physics and Astronomy, Rutgers University, New Brunswick, New Jersey 08903, USA

K.-H. Speidel
Helmholtz-Institut für Strahlen- und Kernphysik, Universität Bonn, D-53115 Bonn, Germany

D. A. Torres
Departamento de Física, Universidad Nacional de Colombia, Bogotá D.C., Colombia

K. Sieja
Université de Strasbourg, IPHC, CNRS, UMR7178, F-67037 Strasbourg, France

M. McCleskey,† A. Cudd, M. Henry, A. Saastamoinen, M. Slater, A. Spiridon, S. Yu. Torilov,‡ and V. I. Zherebchevsky‡
Cyclotron Institute, Texas A&M University, College Station, Texas 77843, USA

G. Gürdal and S. J. Q. Robinson
Physics Department, Millsaps College, Jackson, Mississippi 39210, USA

S. D. Pain
Physics Division, Oak Ridge National Laboratory, Oak Ridge, Tennessee 37831, USA

J. T. Harke
Lawrence Livermore National Laboratory, Livermore, California 94551, USA
(Received 12 March 2014; revised manuscript received 5 May 2014; published 10 June 2014)

Background: The ${}^{88}_{38}$Sr and ${}^{90}_{40}$Zr nuclei have been utilized as closed cores for large-scale shell-model calculations in the $28 \leqslant Z \leqslant 50$ region around the $N = 50$ shell. Measurements of magnetic moments for nuclei in this region would provide microscopic information about the use of ^{88}Sr and ^{90}Zr as stable closed-core nuclei. While the g factors of the 2_1^+ states in the stable Sr isotopes have been previously measured, experimental g factors for the radioactive ^{82,90}Sr have not been obtained to date.
Purpose: The purpose was to measure the g factors of the 2_1^+ and 4_1^+ states in the unstable ^{82}Sr and ^{90}Sr nuclei in order to extend the systematics along the Sr isotopic chain. A comparison of the structure of the $N = 52$ isotopes ^{90}Sr and ^{92}Zr will shed light on the relative robustness of proton subshell closures at $Z = 38$ and $Z = 40$.
Methods: The pickup reaction of α particles in inverse kinematics together with the transient field technique were applied to beams of ^{78}Kr and ^{86}Kr at the Cyclotron Institute of Texas A&M University.
Results: The values $g(^{82}\mathrm{Sr}; 2_1^+) = +0.44(19)$, $g(^{82}\mathrm{Sr}; 4_1^+) = +0.53(39)$, $g(^{90}\mathrm{Sr}; 2_1^+) = -0.12(11)$, and $g(^{90}\mathrm{Sr}; 4_1^+) = -0.02(17)$ were measured for the first time. Simultaneously, the g factors of the low-lying states in the Coulomb-excited beam projectiles were remeasured. The $g(4_1^+) = +1.03(14)$ in ^{86}Kr was also measured for the first time.
Conclusions: For ^{82}Sr both g factors are in agreement with the collective value Z/A expected for nuclei in the middle of a major shell. The g factors in ^{90}Sr are negative but smaller than in the isotone ^{92}Zr. The results also indicate that ^{88}Sr is a proton-soft core nucleus and perhaps even softer than ^{90}Zr.

DOI: 10.1103/PhysRevC.89.064305 PACS number(s): 21.10.Ky, 25.70.De, 25.70.Hi, 27.50.+e

I. INTRODUCTION

The systematics of nuclei within isotopic chains around the closed neutron shell $N = 50$ are of longstanding interest [1,2]. Studies of trends in excitation energies and reduced transition probabilities have been carried out on even-even nuclei with $28 \leqslant Z \leqslant 40$ [3,4]. The energies of the 2_1^+ and 4_1^+ states in the Kr, Sr, and Zr isotopes increase monotonically with increasing neutron number and reach a maximum at $N = 50$. The values of the reduced $E2$ transition probabilities,

*kum@physics.rutgers.edu
†Present address: Department of Radiation Oncology, University of Maryland School of Medicine, Baltimore, Maryland 21201, USA.
‡On leave from Laboratory of Nuclear Reactions, Saint Petersburg State University, Saint Petersburg 199034, Russia.

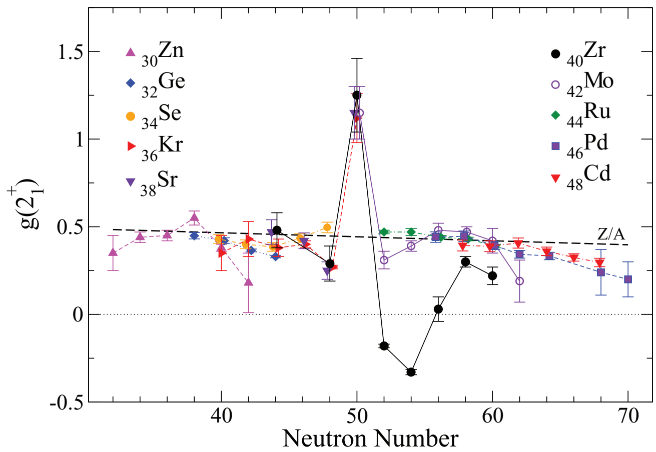

FIG. 1. (Color online) The $g(2_1^+)$ factors of isotopic chains on both sides of the closed neutron shell $N = 50$. The Z/A line represents an average value for the given range of nuclei.

$B(E2; 2_1^+ \rightarrow 0_1^+)$ and $B(E2; 4_1^+ \rightarrow 2_1^+)$, show a marked decrease with the corresponding increase in neutron number, with values consistent with collective excitations below $N = 44$ and with single-particle magnitudes above $N = 44$. Furthermore, all these values for Kr, Sr, and Zr are remarkably similar.

Studies of Sr and Zr nuclei [5–9] have raised the central question of whether $^{88}_{38}$Sr or $^{90}_{40}$Zr should be considered as the closed core for shell-model (SM) calculations. Measurements of magnetic moments of 2_1^+ and 4_1^+ in ^{92,94}Zr [10] have already shown that proton excitations play an important role. The magnetic moment of the 2_1^+ state in $^{90}_{38}$Sr$_{52}$, the isotone of $^{92}_{40}$Zr$_{52}$, could answer the question of whether ^{88}Sr or ^{90}Zr is a better closed-core nucleus.

A compilation of the g factors of the first 2^+ states from $_{30}$Zn to $_{48}$Cd is shown in Fig. 1. At the shell closure $N = 50$, the positive large g factors indicate dominant single-particle proton states, while away from this closed neutron shell, both protons and neutrons contribute to the wave functions. As a matter of fact, most $g(2_1^+)$ factors are close to the collective value of Z/A, although significant deviations in certain isotopic chains were partially explained by SM calculations. But Zr with 40 protons clearly stands out. Adding neutrons beyond $N = 50$ results in negative g factors. Obviously, neutron excitation dominates in the structure of these excited Zr states. If this effect were simply attributed to a $1p_{1/2}$ subshell closure for protons at $Z = 40$, a similar behavior might be expected for the neighboring Sr isotopes since at $Z = 38$ the proton $1p_{1/2}$ orbital is empty and the $0f_{5/2}$ and $1p_{3/2}$ orbitals are completely filled.

Only the three stable ^{84,86,88}Sr isotopes have had magnetic moments measured [11,12]. The present investigation focuses on the measurements of magnetic moments of 2_1^+ and 4_1^+ states in the outlying unstable ^{82,90}Sr isotopes. Radioactive beams of Sr isotopes are not yet available. However, α-capture from ^{12}C by stable beams of ^{78,86}Kr populates states in ^{82,90}Sr.

The α-transfer reaction has been observed in nuclei as light as S [13] and has been used for many studies ranging from lighter nuclei such as ^{62}Zn [14] to the heaviest one investigated so far, ^{100}Pd [15]. While the details of the α-transfer reaction are not yet well described and even less understood, nevertheless, the body of measurements has proved to be coherent and robust.

As part of the study, the Coulomb excitation of the ^{78,86}Kr beams was also examined, both for internal calibration purposes and for a determination of the magnetic moment of the 4_1^+ state in ^{86}Kr, which had not been measured previously. In addition, from experiments carried out at three beam energies, a qualitative measure of the excitation cross section for the α-capture reaction as a function of energy was obtained.

II. THE EXPERIMENT

The transient-field (TF) technique in inverse kinematics was applied to measure the magnitude and sign of g factors of short-lived excited states using the perturbed angular correlation method. The probe ions were Coulomb excited and spin aligned on a light target material. They subsequently traverse a polarized ferromagnetic layer where the spin precession occurs and, finally, stop in a field-free environment. Simultaneously, when the projectile energies exceed the Coulomb barrier for the light target nuclei, pickup reactions lead to excited nuclei suitable for TF measurements.

Isotopically pure ^{78}Kr and ^{86}Kr beams at an average intensity of $\sim$1 pnA were delivered by the K500 Texas A&M University (TAMU) cyclotron. Two experiments were performed. For the first experiment a beam energy of 3.2 MeV/u was chosen. This energy is above the Coulomb barrier by 9% for ^{86}Kr on ^{12}C and by 6% for ^{78}Kr on ^{12}C. It was found that the yield for the α-transfer reaction with ^{78}Kr was

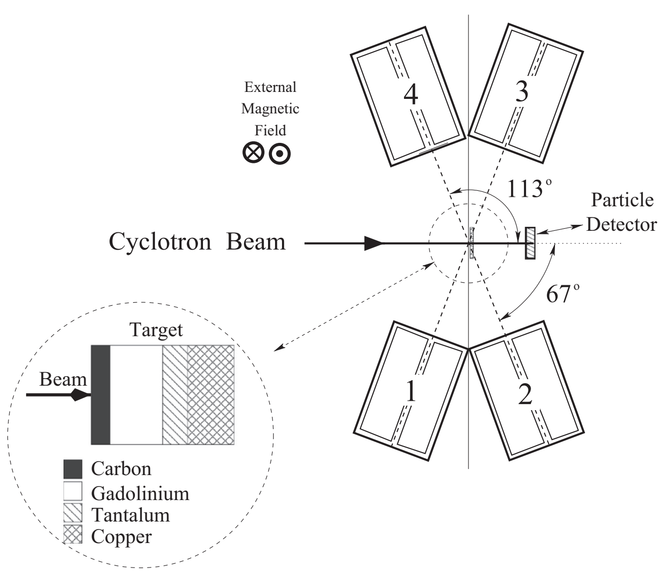

FIG. 2. Experimental setup. Four clover HPGe γ detectors and a circular (300 mm^2) PIPS Canberra silicon surface-barrier particle detector were located symmetrically around the target. Clovers 2 and 3 were placed in the forward hemisphere at $\pm 67^\circ$, while clovers 1 and 4 occupied the backward angles at $\pm 113^\circ$, all at a distance of 120 mm from the target. The particle detector was positioned 20 mm downstream of the target at 0° to the beam direction and spanned an opening angle of $\pm 24^\circ$. Inset: The multilayered target design.

TABLE I. Composition of the targets used in these experiments. All thicknesses are given in mg/cm^2. Additional copper foils of 5.6 mg/cm^2 were placed behind the target and in front of the particle detector to prevent the beam from reaching the detector.

Target	C	Gd	Ta	Cu
I	0.9	5.096	1.1	5.03
II	0.62	6.109	1.0	4.84

about 3 times higher than that with ^{86}Kr. Therefore, in the second experiment ^{86}Kr was run at the lower energies of 3.1 and 3.0 MeV/u. The α-transfer yields indeed increased upon lowering the beam energy. A qualitative measure of the excitation via α transfer was obtained and is discussed below.

The experimental setup is similar to that used in former experiments carried out at WNSL, Yale University. A schematic is presented in Fig. 2.

The composition of the multilayered targets [16] is reported in Table I. Target I was used at 3.2 MeV/u, while target II was used in the second experiment.

Both the Coulomb excitation of beam projectiles and the α transfer to the beam occur in the carbon layer. The reaction products move forward and traverse the gadolinium and tantalum layers. While the heavier reaction products are stopped in the copper layer of the target, the lighter products – carbon nuclei, α particles, and protons – reach the particle detector.

The target was mounted on the tip of a Displex Closed Cycle refrigerator, which serves as one pole piece of an electromagnet. An external magnetic field of 0.07 T was large enough to saturate the gadolinium layer of the target. The field direction was reversed every 130 s. The target was

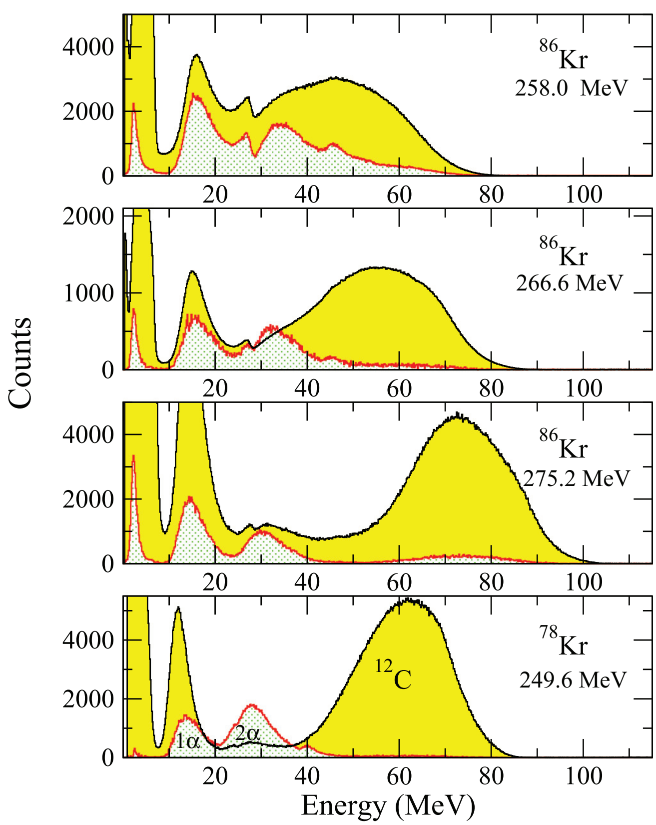

FIG. 3. (Color online) Particle spectra and overlaid spectra of particles in coincidence with γ transitions in ^{90}Sr and ^{82}Sr at the three beam energies. The lightly shaded areas show ΔE spectra of α particles. At the lower beam energies the spectra of the Coulomb-scattered carbon ions and α particles overlap more and more. The "cusps" in the spectra are artifacts due to the finite thickness of the particle detector.

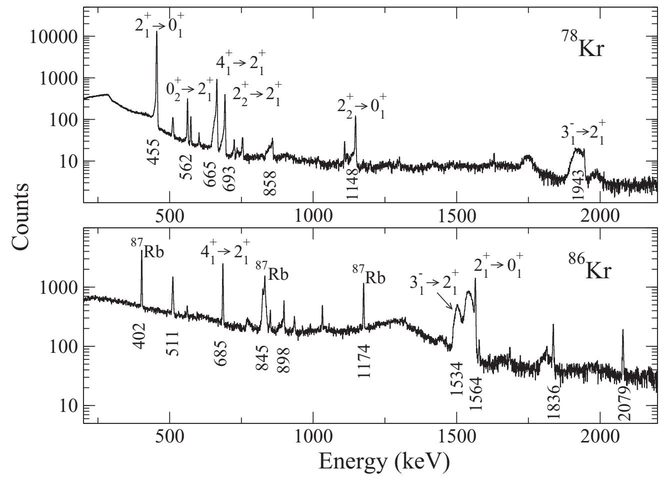

FIG. 4. Random-subtracted γ-ray spectra in coincidence with forward-scattered carbon particles recorded in a clover segment at $\theta = 121^\circ$. The ^{87}Rb lines in the ^{86}Kr spectrum arise from the proton pickup reaction ^{12}C(^{86}Kr,^{11}B)^{87}Rb, where ^{11}B is indistinguishable from ^{12}C in the particle spectrum.

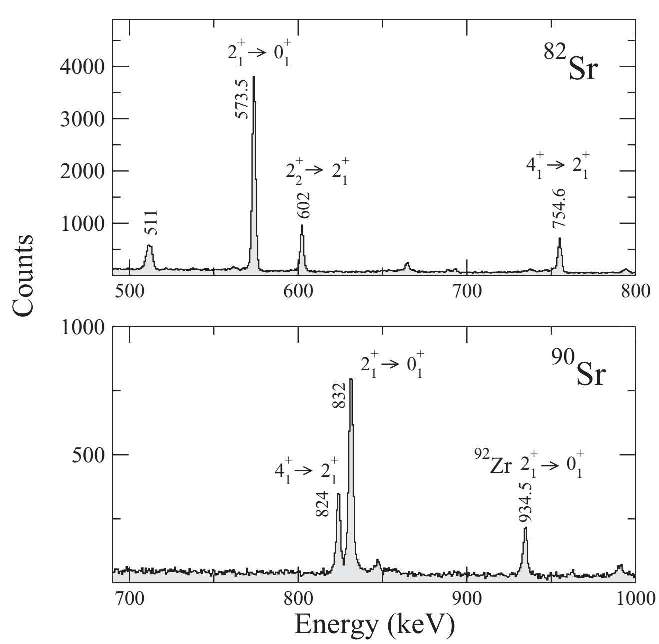

FIG. 5. Random-subtracted γ-ray spectra in coincidence with the double α peak in the particle spectra showing the transitions in ^{82}Sr and ^{90}Sr. ^{92}Zr is populated in the ^{12}C(^{86}Kr,α2n)^{92}Zr reaction.

kept at a temperature of about 50 K during the precession measurements.

The preamplifier output signals of the particle and γ detectors were digitized using a PIXIE-4 digital pulse-processing multichannel data acquisition system from XIA [17]. The energies and times were recorded as singles events, from which off-line event files for particles and γ's with a time difference of less than ± 2 μs were selected. The γ energies of all 16 clover segments were gain matched and Compton addback was performed for each segment in a clover.

In Fig. 3 particle spectra associated with both the Coulomb excitation of the beam and the α transfer are shown. Appropriate gates on time and on γ energies were applied to produce the α-particle spectra.

The particle spectrum associated with the α-transfer reaction shows two peaks related to the detection of either both α particles or only one from the ^{8}Be breakup. The particle detector is 100 μm thick. Neither α particles ($\sim$40 MeV) nor other light particles stop in the detector.

In Figs. 4 and 5 partial γ spectra are shown. In the data analysis each clover segment (germanium crystal) was treated as a separate detector.

III. MAGNETIC MOMENT MEASUREMENT

The magnetic moment of a given state is determined from the measurement of the precession of this moment in the TF magnetic hyperfine field while the ions traverse the ferromagnetic foil. The precession gives rise to a rotation of the particle-γ angular correlation. This rotation is obtained from the change in the intensity of the particle-γ coincidence rate as the direction of the magnetic field at the target is changed from up to down with respect to the plane defined by the γ detectors. As fully described in Ref. [18], the precession angle $\Delta\theta = \epsilon / S(\theta)$ is derived from double-counting-rate ratios ϵ in the four γ detectors. The logarithmic slope $S(\theta) = \frac{1}{W(\theta)} \cdot \frac{dW}{d\theta}$ is calculated from the measured angular correlation

$$W(\theta) = 1 + A_2 \cdot Q_2 \cdot P_2(\cos\theta) + A_4 \cdot Q_4 \cdot P_4(\cos\theta). \quad (1)$$

Here the $P_k(\cos\theta)$ are the Legendre polynomials of degree k, the A_k are the experimental angular-correlation coefficients, which depend on the multipolarity of the γ-ray transition, and the Q_k are the geometrical attenuation coefficients accounting for the finite solid angle of the γ detectors.

The particle-γ correlations were determined from anisotropy ratios. In a dedicated set of measurements opposite detector pairs were set at 50° and 80°, respectively, in their specific quadrants, and anisotropy double-ratios, like those used for the precession measurement, were calculated. Anisotropy ratios were also derived from the granularity of the clover segments at the precession angles. The precise location of the individual clover segments was determined from detector scans with a collimated ^{137}Cs source. The relative energy efficiencies of the segments were measured with a ^{152}Eu source at the target position and checked with isotropic γ lines in the precession data.

In the γ-detection plane two clover segments are separated by 16°. When using the higher statistics precession data, ratios of the sums of the up and down γ-line intensities in each clover detector segment, corrected for relative detection efficiencies, were used to form anisotropy ratios. The intensity ratios for the 59°/75° and 121°/103° data are in all cases >1, confirming spin alignment even from the weak α-γ correlations. Examples of measured angular correlations are shown in Fig. 6.

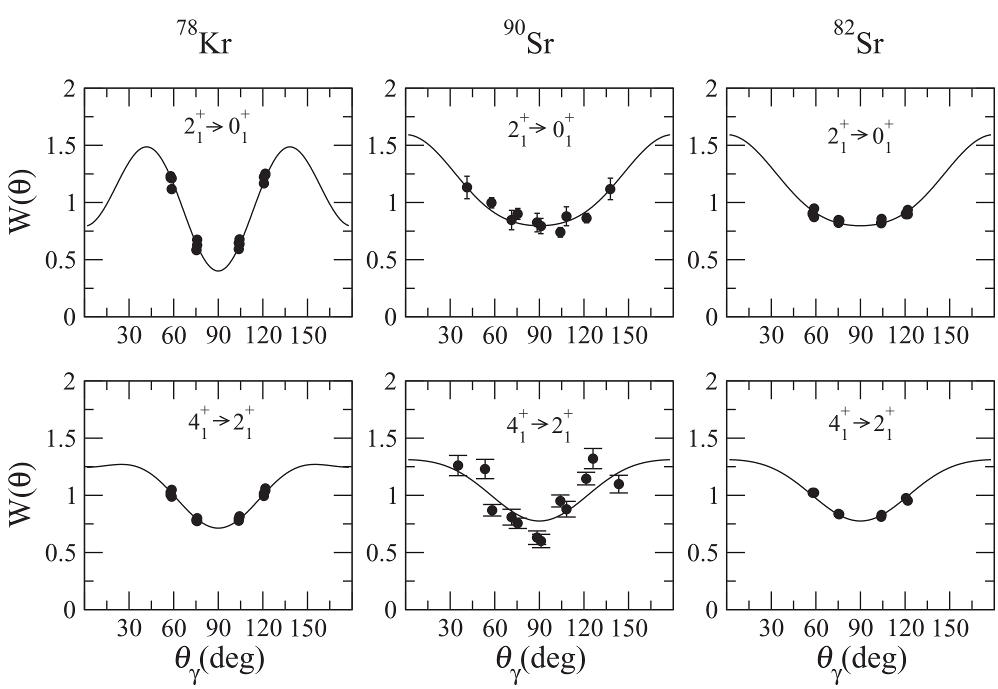

FIG. 6. Angular correlations for Coulomb excitation and α transfer derived from precession data in clover segments. The α-transfer data for ^{90}Sr also include data for clover detectors positioned at 50°, 80°, 100°, and 130°.

TABLE II. Summary of the kinematic parameters for the transient-field measurement. $\langle E\rangle_{\text{in}}$ and $\langle E\rangle_{\text{out}}$, and $\langle v/v_0\rangle_{\text{in}}$ and $\langle v/v_0\rangle_{\text{out}}$, are, respectively, the average energies and velocities of the excited probe ions as they enter into, and exit from, the gadolinium layer; $v_0 = e^2/\hbar$ is the Bohr velocity. The values are calculated for the 2_1^+ states, at the given beam energies and for the different targets. T_{eff}, the effective transit time of the ions through the ferromagnetic layer, takes into account the decay in flight, which is important for the short-lived states.

	E_{Beam}		Target	$\langle E\rangle_{\text{in}}$	$\langle E\rangle_{\text{out}}$	$\langle \frac{v}{v_0}\rangle_{\text{in}}$	$\langle \frac{v}{v_0}\rangle_{\text{out}}$	T_{eff}
	(MeV/u)	(MeV)		(MeV)	(MeV)			(fs)
^{78}Kr	3.2	249.6	I	106	26	7.4	3.7	548
^{82}Sr			I	119	33	7.6	4.0	508
^{86}Kr	3.2	275.2	I	130	43	7.8	4.5	228
^{90}Sr			I	141	49	7.9	4.7	461
^{86}Kr	3.1	266.6	II	137	35	8.0	4.0	274
^{90}Sr			II	149	41	8.2	4.3	564
^{86}Kr	3.0	258.0	II	132	32	7.9	3.9	278
^{90}Sr			II	143	38	8.0	4.1	581

The α-transfer reaction populates the nuclear states more uniformly and with little alignment. The angular correlation is attenuated and the logarithmic slopes are less than a quarter of the typical slopes for Coulomb excitation, which severely constrains the sensitivity of the precession measurements and can only be compensated for by higher counting statistics.

The kinematic parameters relevant to this experiment are compiled in Table II. The results of the precession measurements are listed in Table III.

IV. RESULTS

Below the Coulomb barrier the Coulomb excitation of the beam projectiles is the dominant reaction channel. At higher energies, fusion evaporation reactions take over and flood the particle detector with high-energy light particles. These particles do not stop in the detector but produce the intense low-energy peak in the particle spectra. As more reaction channels open up the Coulomb excitation channel is increasingly suppressed.

The α pickup is a resonance-like process near the Coulomb barrier. In earlier measurements it was found that the onset of α transfer is already observed at beam energies just below the Coulomb barrier. In order to obtain an excitation yield for the α transfer at the three ^{86}Kr beam energies, in the absence of a beam current integration, the yield of Coulomb-excited Gd γ rays in the target was used for normalization. The Coulomb excitation of Gd by Kr occurs well below the barrier and its energy dependence was calculated. In Fig. 7 the relative yields for the Coulomb excitation of the beam particles and α-transfer reactions are shown for ^{86}Kr at three beam energies. The Coulomb excitation yield was derived from the intensity of the combined γ peaks at 1534 and 1564 keV (Fig. 4). The α-transfer yield was taken from the sum of the 824 and 832 keV γ lines in ^{90}Sr (Fig. 5). The data in Fig. 7 indicate that the α-pickup cross section decreases rapidly at higher beam energies. It should be noted that the beam loses about 30 MeV of its energy in the carbon layer of the target and that therefore a more quantitative analysis cannot be made.

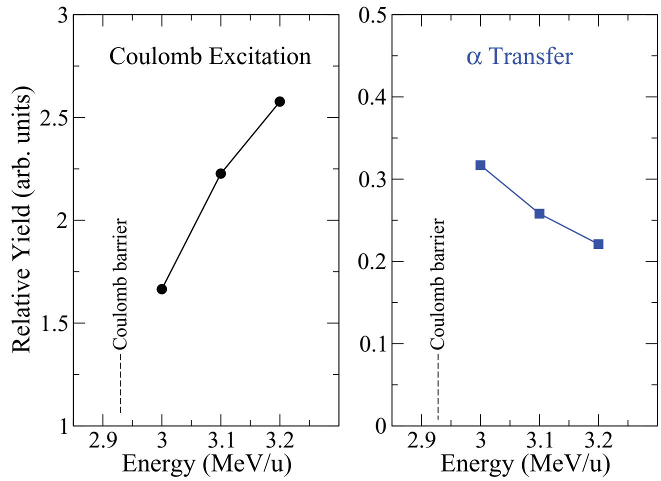

FIG. 7. (Color online) Energy dependence of the yields for Coulomb excitation and α transfer with ^{86}Kr beams.

A. ^{78}Kr

The dominant feature in the de-excitation of ^{78}Kr is the $2_1^+ \to 0_1^+$ transition. Feeding from the 4_1^+, 2_2^+, and 3_1^- states is negligible. The g factors obtained in this work are in excellent agreement with the earlier measurement [20]. A comparison is reported in Table III. In the older measurements the light target layer was ^{26}Mg and the beam energy was below the Coulomb barrier (less feeding). The new results have slightly better statistical errors.

B. ^{86}Kr

The $g(2_1^+)$ factor was also measured before [20]. In that previous experiment the same target was used as for ^{78}Kr. The beam energy[1] of 2.67 MeV/u was well below the Coulomb barrier of 2.87 MeV/u on ^{26}Mg. At that energy, only the 2_1^+ state was excited and four 5 × 5-in. NaI crystals were used to detect the γ rays. In the present experiments the ^{86}Kr beam energies were above the Coulomb barrier (2.93 MeV/u on C) and the 4_1^+ and 3_1^- states, which decay into the 2_1^+ state, were increasingly excited. The $g(4_1^+) = +1.03(14)$ was never measured before.

The γ line of the $2_1^+ \to 0_1^+$ transition cannot be individually analyzed. As shown in Fig. 4 (^{86}Kr), the 1564 keV γ line is fully Doppler shifted. The 2_1^+ state has a very short lifetime of $\tau = 0.44$ ps. The feeding by the 4_1^+ state, due to its long lifetime of $\tau = 4.5$ ns, contributes the stopped part of the $2_1^+ \to 0_1^+$ γ line. The 1534 keV decay γ rays of the 3_1^- state are also fully Doppler shifted, setting an upper limit of 300 fs on its lifetime.

Especially at the forward precession angles the different components, the 2_1^+, 3_1^-, and 4_1^+ decay γ lines, overlap and

[1]In Ref. [20] the beam energy was incorrectly reported for ^{86}Kr in Table I. The correct value is 229.6 MeV.

TABLE III. Experimental results for states in ^{78,86}Kr and ^{82,90}Sr. Also included are the slopes for full clovers and precession angles. $\Delta\theta(g=1)$ was calculated using the Rutgers parametrization [19]. The lifetimes are taken from the National Nuclear Data Center (NNDC) data base [4].

	E_{Beam}	I_i^π	E_γ	τ	$\Delta\theta(g=1)$	$\lvert S(67^\circ)\rvert$	$\Delta\theta$	g	
	MeV/u		(keV)	(ps)	(mrad)	(mrad^{-1})	(mrad)	This work	Ref. [20]
^{78}Kr									
	3.2	2_1^+	455.0	31.3	50.4	2.04(2)	22.4(4)	+0.45(2)	+0.43(3)
		4_1^+	665.0	3.49	46.7	0.80(3)	23.1(22)	+0.48(5)	+0.46(7)
		2_2^+	1147.0	5.34	46.0	1.71(4)	25.5(28)	+0.55(7)	+0.54(10)
^{86}Kr									
	3.2	2_1^+	1564.8	0.44	22.2	1.36(5)	22.9(15)	+1.03(6)	
	3.1				26.9	1.48(1)	29.9(17)	+1.11(10)	
	3.0				26.8	1.58(5)	31.9(15)	+1.19(8)	
	Weighted mean							+1.10(5)	+1.12(14)
	3.2	4_1^+	685.3	4.5 ns	46.7	0.90(20)	42.3(101))	+0.91(22)	
	3.1				57.3	0.85(15)	71.1(150)	+1.24(27)	
	3.0				58.3	0.75(15)	58.2(152)	+1.00(27)	
	Weighted mean							+1.03(14)	
^{82}Sr									
	3.2	2_1^+	573.5	12.8	50.3	0.29(4)	22.2(94)	+0.44(19)	
		4_1^+	754.9	1.44	40.2	0.55(6)	21.4(157)	+0.53(39)	
^{90}Sr									
	3.2	2_1^+	831.7	10.1	47.0	0.39(4)	−7.6(140)	−0.16(30)	
	3.1				57.6		−0.9(118)	−0.02(20)	
	3.0				58.5		−9.4(88)	−0.16(15)	
	Weighted mean							−0.12(11)	
	3.2	4_1^+	824.2	17.3	47.0	0.56(10)	−1.2(112)	−0.03(25)	
	3.1				57.6		3.5(221)	+0.06(38)	
	3.0				58.5		−3.6(168)	−0.06(28)	
	Weighted mean							−0.02(17)	

cannot be separated. Since a measurement of $g(2_1^+)$ was not a primary goal, only the spectra of the two backward detectors, where the 3_1^- γ line was well separated, were analyzed. The slopes and results are listed in Table III for the three beam energies. The weighted mean is in agreement with the literature value of $g(2_1^+)$. When the forward detectors are included in the analysis, the result is the same within the errors, which is not surprising, since $g(4_1^+) \sim g(2_1^+)$. The $3_1^- \to 2_1^+$ transition contributes a negligible precession effect because the lifetime of the 3_1^- state is short and the slope of an $E1$ angular correlation at 67° is small.

The reproduction of the earlier Kr measurements confirms the calibration of the TF and strengthens the confidence in the current data, an especially reassuring fact when, as in the case of ^{90}Sr, small effects are to be expected.

C. ^{82}Sr

Clean ^{82}Sr γ spectra can be produced by gating on the double-α-peak region in the particle spectra (see Fig. 3). Some additional intensity in the ^{82}Sr lines was obtained by extending the gate to include the single α peak.

D. ^{90}Sr

The particle gates have to be chosen carefully to obtain clean ^{90}Sr γ spectra with low background. Although at the lower beam energies (Fig. 3) the α-transfer reaction is enhanced, the Coulomb-scattered carbon ions have less energy and therefore overlap with the double α peak. Furthermore, the α particles are more spread out in the spectra. A clean separation of the different reaction channels is not possible. In addition,

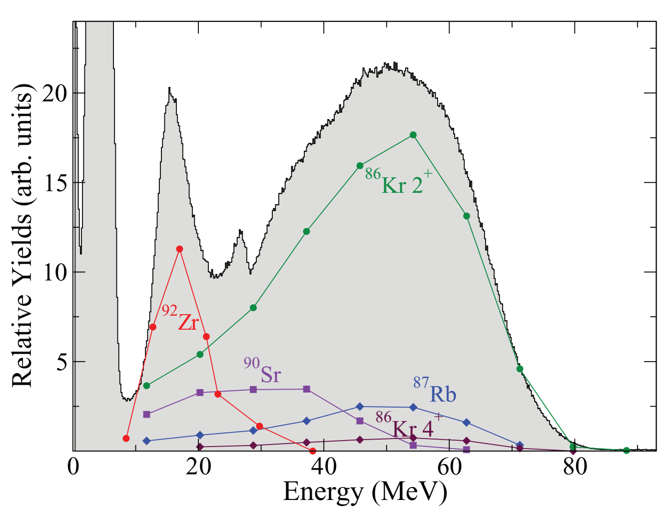

FIG. 8. (Color online) Corresponding particle yields for the main reaction channels obtained with the 3.0-MeV/u ^{86}Kr beam. The graph for ^{86}Kr 2_1^+ is scaled down by a factor of 6.

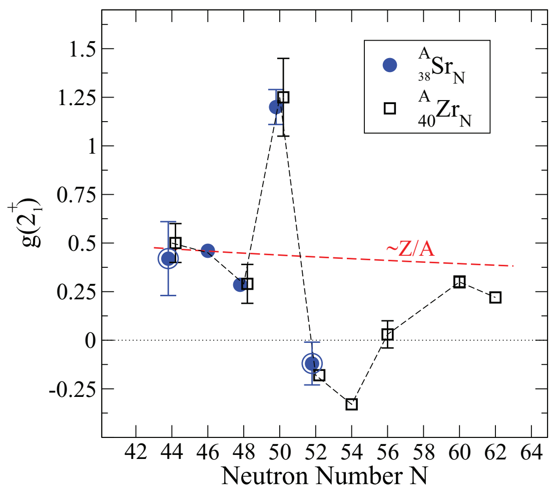

FIG. 9. (Color online) Comparison of the g factors in the Zr and extended Sr isotopic chains. The new results ($N = 44, 52$) are highlighted. Missing error bars are smaller than the symbol size.

with the ^{86}Kr beam a significant one-proton pickup to ^{87}Rb occurs. This ^{12}C(^{86}Kr,^{11}B)^{87}Rb reaction, as well as a strong ^{12}C(^{86}Kr,α2n)^{92}Zr reaction, were observed. Neither reaction channel was seen with the ^{78}Kr beam (see Fig. 4).

The various overlapping particle yields and their energy dependences are shown in Fig. 8. The relative yields were obtained from the intensities of the respective γ lines in spectra gated by particle slices. The strong proton pickup may be related to the $N = 50$ structure of ^{86}Kr. The ^{11}B nuclei overlap with the α particles (see ^{87}Rb and ^{90}Sr in Fig. 8) in the particle spectra. The 845 keV γ line of the $\frac{1}{2}^- \rightarrow \frac{3}{2}^-_{g.s.}$ transition in ^{87}Rb, $\tau = 146(10)$ fs [21], is fully Doppler shifted and interferes with the 824/832 keV lines of ^{90}Sr in the backward detectors for particles with more than 40 MeV.

The experimental results for ^{78}Kr, ^{86}Kr, ^{82}Sr, and ^{90}Sr are summarized in Table III and the new Sr results are added to the systematics of the previously obtained Sr and Zr g factors in Fig. 9.

V. DISCUSSION AND THEORY

The present measurements encompass three distinct regions, $42 \leqslant N \leqslant 46$, in the middle of a major shell where collectivity dominates the structure, $N = 50$, characteristic of closed-shell nuclei, and $N = 52$, the onset of the next major shell. The isotonic pairs of $_{38}$Sr and $_{40}$Zr isotopes have very similar structures. The main difference between them is that in Sr the proton $p_{1/2}$ orbital is empty, while in Zr it is filled. As a result, the low-lying states have almost-equal values of excitation energies, reduced transition probabilities, and magnetic moments [12]. The measured g factors of the 2_1^+ and 4_1^+ states in ^{82}Sr, ^{84}Sr, and ^{84}Zr are $g(^{82}\text{Sr};2_1^+) = +0.44(19)$, $g(^{82}\text{Sr};4_1^+) = +0.53(39)$, $g(^{84}\text{Zr};2_1^+) = +0.48(10)$, and $g(^{84}\text{Zr};4_1^+) = +0.51(23)$ [22], all close to $\sim Z/A$, reflecting collective structures.

The structure of nuclei with $N = 50$ is expected to reflect mainly proton excitation. In ^{86}Kr both 2_1^+ and 4_1^+ states exhibit large g factors, $g(^{86}\text{Kr};2_1^+ = +1.10(5)$ and $g(^{86}\text{Kr};4_1^+ = +1.03(14)$, comparable to the $g(2_1^+)$ values observed in the neighboring ^{88}Sr, ^{90}Zr, and ^{92}Mo nuclei of +1.20(9) [11,12], +1.25(21) [23], and +1.15(14) [24], respectively. These numbers agree well with +1.35, the Schmidt value for protons excited into the $g_{9/2}$ orbital, calculated with an effective $g_s^{\text{eff}} = 0.75 g_s^{\text{free}}$ [25].

The g factors of the 2_1^+ states in the $N = 52$ isotopes, ^{90}Sr and ^{92}Zr, are smaller than those of the neighboring even-odd nuclei with $N = 51$, $g(^{89}\text{Sr};5/2^+) = -0.459$ and $g(^{91}\text{Zr};5/2^+) = -0.52$ [4], which are close to the effective g factor of a $d_{5/2}$ neutron, −0.57. From a simple SM perspective, the addition of another neutron in the $d_{5/2}$ orbital should not change the g factor.

TABLE IV. Excitation energies (in MeV) and magnetic moments (in n.m.) obtained for ^{90}Sr in shell-model calculations based on a ^{78}Ni core. Proton and neutron contributions to the magnetic moment are listed separately.

J^π	E	μ	μ_p	μ_n
2_1^+	0.93	−0.18	0.45	−0.63
4_1^+	1.63	−1.36	0.33	−1.69

SM calculations for ^{90}Sr and ^{86}Kr have been performed in a model space outside the ^{78}Ni core containing the proton $0f_{5/2}$, $1p_{3/2}$, $1p_{1/2}$, $0g_{9/2}$ and the neutron $1d_{5/2}$, $0g_{7/2}$, $1d_{3/2}$, $2s_{1/2}$, $0h_{11/2}$ orbitals. The effective interaction for this valence space has been constructed by monopole corrections of the realistic G matrices based on the CD-Bonn potential [26,27]. Details of this procedure can be found in [2]. The interaction has been previously employed in a large number of studies of neutron-rich nuclei with $Z = 32$–40 and $N = 52$–56 (see, e.g., [28–30]). In particular, it has been successful in the description of excitation energies of $^{92–96}$Sr isotopes [31].

The Hamiltonian matrices' diagonalization in the complete model space has been achieved with the j-coupled code NATHAN [32]. In the calculations of magnetic moments, a standard M1 operator has been used with the 0.75 quenching of spin g factors.

The results of SM calculations for ^{90}Sr are summarized in Table IV, where the excitation energies and magnetic moments of the lowest excited states are listed. The total contributions of protons and neutrons to the magnetic moments are given individually. As reported in Table V, fair agreement is found between theoretical and experimental results. The SM correctly predicts the sign and magnitude of the magnetic moments; however, the absolute value for the 4_1^+ state is

TABLE V. Comparison of experimental (Expt.) g factors with results of large-scale shell-model calculations using a ^{78}Ni core.

	$N = 50$		$N = 52$			
	$^{86}_{36}$Kr (this work)		$^{90}_{38}$Sr (this work)		$^{92}_{40}$Zr (published)	
	Expt.	SM	Expt.	SM	Expt. [10]	SM [2]
$g(2_1^+)$	+1.10(5)	+1.03	−0.12(11)	−0.09	−0.18(1)	−0.24
$g(4_1^+)$	+1.03(14)	+0.99	−0.02(17)	−0.34	−0.50(11)	−0.43

slightly overestimated. One should note that the final value of the magnetic moment results from a cancellation between the large negative value for neutrons and the smaller positive contribution from the proton part. The nonzero proton contribution comes from the excitations of the $f_{5/2}$ and $p_{3/2}$ protons to the $p_{1/2}$ and $g_{9/2}$ shells, whose summed occupation is 1.3 particles in the 2_1^+ and 1.25 particles in the 4_1^+ state. The amplitude of the neutron contribution is maximal when the two neutrons occupy the $d_{5/2}$ shell. The $d_{5/2}$ occupation obtained in these configuration-mixing calculations is large: 1.75 particles in the 2_1^+ and 1.9 particles in the 4_1^+. The fact that, instead of 2, only 1.75 neutrons in the $d_{5/2}$ shell are sufficient to account for the g factor of the 2_1^+ state suggests that neutron-neutron interactions probably also contribute to the reduction of the g factor. Something similar has been observed in the $0d_{5/2}$ shell in oxygen isotopes. Their measured $g(^{17}\mathrm{O};5/2^+) = -0.7575$ and $g(^{18}\mathrm{O};2_1^+) = -0.29$ were reproduced in calculations with the USD interaction [33] in the *sd* shell with neutrons only ($g = -0.65$ and $g = -0.35$, respectively), implying that neutron-neutron interactions are responsible for this effect.

^{88}Sr has been previously used as a doubly magic core in SM calculations for Zr isotopes [5]. However, it has been suggested in Ref. [2] that the proton excitations are important in the description of the low-lying excited states in this region. In the latter SM calculations using the ^{78}Ni core, ^{88}Sr is predicted to have 60% of the closed-shell configuration in its ground state. In comparison with the results with a ^{78}Ni core presented in Table IV, the calculations with the ^{88}Sr core and the interaction from Ref. [5] give larger negative values of the magnetic moments in ^{90}Sr ($-0.31\mu_N$ for the 2_1^+ and $-1.90\mu_N$ for the 4_1^+), confirming further the non-negligible role of the proton excitations across the $Z = 38$ gap that are included when a ^{78}Ni core is used.

The SM calculations using the ^{78}Ni core and the extended model space yield, for ^{86}Kr, $g(2_1^+) = +1.03$ and $g(4_1^+) = +0.99$. All these results are in good agreement with the measured g factors. The experimental data and the SM calculations are summarized in Table V.

VI. SUMMARY

Magnetic moment measurements of the 2_1^+ and 4_1^+ states were carried out in ^{82}Sr and ^{90}Sr nuclei, which extend the Sr isotopic chain on both sides of the line of stability. The isotopes were populated by the α-transfer reaction from a ^{12}C target to beams of stable ^{78}Kr and ^{86}Kr.

The lighter ^{82}Sr, with $N = 44$ neutrons, lies in the middle of a major neutron shell. Collectivity is therefore expected to characterize its structure. In contrast, for the heavier ^{90}Sr, lying above the line of stability, with two neutrons beyond the magic $N = 50$ shell, single-particle degrees of freedom should be the dominating feature of the nuclear structure. Both these expectations have been confirmed by the present experiments.

The values of the g factors of the 2_1^+ and 4_1^+ states in ^{90}Sr provide information about the integrity of ^{88}Sr as a closed-core nucleus. The observed negative magnetic moments indeed confirm the expected dominance of neutrons in the structure of these states; however, the smaller-than-expected measured g-factor values suggest that the ^{88}Sr core proton excitations also play an important role. The same arguments were used before [10] to explain the measured moments for the 2_1^+ and 4_1^+ states in ^{92}Zr. Furthermore, the comparison of the measured values of the 4_1^+ states of ^{90}Sr and ^{92}Zr [with the magnitude of the negative $g(4_1^+)$ factor of ^{92}Zr being significantly larger than the corresponding value of ^{90}Sr] indicate that ^{88}Sr is a proton-soft core nucleus and probably even softer than ^{90}Zr. The present and former SM calculations for these two nuclei are generally in good agreement with these observations, as demonstrated by the close reproduction of the experimental $g(2_1^+)$ factors. However, the calculations of the $g(4_1^+)$ factors seem to underestimate the proton contributions, which are manifested in the almost-vanishing experimental $g(4_1^+)$ factor in ^{90}Sr.

As a corollary, and as an additional check on the calibration of the TF, the magnetic moments of the 2_1^+, 4_1^+, and 2_2^+ states in ^{78}Kr were remeasured. In this experiment at the higher beam energies, the 4_1^+ state of ^{86}Kr was also strongly excited and its magnetic moment was measured for the first time.

ACKNOWLEDGMENTS

The experimental work was done at the Texas A&M Cyclotron Institute; the help of local students, postdoctoral fellows, and staff is greatly appreciated. K.-H.S. is grateful for travel support from Rutgers. D.A.T. is thankful for support from COLCIENCIAS Travel Grant No. 613-2013 and for financial support from Universidad Nacional de Colombia and Rutgers. This work was supported in part by the US National Science Foundation, by US Department of Energy Office Grants No. DE-FG02-93ER40773 and No. DE-NA0001785, by Lawrence Livermore National Security, LLCL, under Contract No. DE-AC52-07NA27344, and by the Department of Energy's NNSA Office of Defense Nuclear Nonproliferation Research and Development.

[1] H. Mach, F. K. Wohn, G. Molnar, K. Sistemich, J. C. Hill, M. Moszynski, R. Gill, W. Krips, and D. Brenner, Nucl. Phys. A **523**, 197 (1991).
[2] K. Sieja, F. Nowacki, K. Langanke, and G. Martínez-Pinedo, Phys. Rev. C **79**, 064310 (2009).
[3] S. L. Rice, Y. Y. Sharon, N. Benczer-Koller, G. J. Kumbartzki, and L. Zamick, Phys. Rev. C **88**, 044334 (2013).
[4] ENSDF; http://www.nndc.bnl.gov/nndc/ensdf/
[5] A. Holt, T. Engeland, M. Hjorth-Jensen, and E. Osnes, Phys. Rev. C **61**, 064318 (2000).
[6] E. A. Stefanova, R. Schwengner, G. Rainovski, K. D. Schilling, A. Wagner, F. Dönau, E. Galindo, A. Jungclaus, K. P. Lieb, O. Thelen, J. Eberth, D. R. Napoli, C. A. Ur, G. de Angelis, M. Axiotis, A. Gadea, N. Marginean, T. Martinez, T. Kröll, and T. Kutsarova, Phys. Rev. C **63**, 064315 (2001).

[7] C. Özen and D. J. Dean, Phys. Rev. C **73**, 014302 (2006).
[8] N. Lo Iudice and C. Stoyanov, Phys. Rev. C **73**, 037305 (2006).
[9] V. Werner, D. Belic, P. von Brentano, C. Fransen, A. Gade, H. von Garrel, J. Jolie, U. Kneissl, C. Kohstall, A. Linnemann, A. F. Lisetskiy, N. Pietralla, H. H. Pitz, M. Scheck, K.-H. Speidel, F. Stedile, and S. W. Yates, Phys. Lett. B **550**, 140 (2002).
[10] G. Jakob, N. Benczer-Koller, J. Holden, G. Kumbartzki, T. J. Mertzimekis, K.-H. Speidel, C. W. Beausang, and R. Krücken, Phys. Lett. B **468**, 13 (1999).
[11] A. I. Kucharska, J. Billowes, and M. A. Grace, J. Phys. G **14**, 65 (1988).
[12] G. J. Kumbartzki, K.-H. Speidel, N. Benczer-Koller, D. A. Torres, Y. Y. Sharon, L. Zamick, S. J. Q. Robinson, P. Maier-Komor, T. Ahn, V. Anagnostatou, C. Bernards, M. Elvers, P. Goddard, A. Heinz, G. Ilie, D. Radeck, D. Savran, V. Werner, and E. Williams, Phys. Rev. C **85**, 044322 (2012).
[13] K.-H. Speidel, S. Schielke, J. Leske, J. Gerber, P. Maier-Komor, S. J. Q. Robinson, Y. Y. Sharon, and L. Zamick, Phys. Lett. B **632**, 207 (2006).
[14] O. Kenn, K.-H. Speidel, R. Ernst, S. Schielke, S. Wagner, J. Gerber, P. Maier-Komor, and F. Nowacki, Phys. Rev. C **65**, 034308 (2002).
[15] D. A. Torres, G. J. Kumbartzki, Y. Y. Sharon, L. Zamick, B. Manning, N. Benczer-Koller, G. Gürdal, K.-H. Speidel, M. Hjorth-Jensen, P. Maier-Komor, S. J. Q. Robinson, T. Ahn, V. Anagnostatou, M. Elvers, P. Goddard, A. Heinz, G. Ilie, D. Radeck, D. Savran, and V. Werner, Phys. Rev. C **84**, 044327 (2011).
[16] P. Maier-Komor, K.-H. Speidel, and A. Stolarz, Nucl. Instrum. Methods Phys. Res. A **334**, 191 (1993).
[17] X-Ray Instrumentation Associates; http://www.xia.com/
[18] N. Benczer-Koller and G. J. Kumbartzki, J. Phys. G: Nucl. Part. Phys. **34**, R321 (2007).
[19] N. K. B. Shu, D. Melnik, J. M. Brennan, W. Semmler, and N. Benczer-Koller, Phys. Rev. C **21**, 1828 (1980).
[20] T. J. Mertzimekis, N. Benczer-Koller, J. Holden, G. Jakob, G. Kumbartzki, K.-H. Speidel, R. Ernst, A. Macchiavelli, M. McMahan, L. Phair, P. Maier-Komor, A. Pakou, S. Vincent, and W. Korten, Phys. Rev. C **64**, 024314 (2001).
[21] C. Stahl, J. Leske, N. Pietralla, P. R. John, G. Rainovski, J. Gerl, I. Kojouharov, and H. Schaffner, Phys. Rev. C **87**, 037302 (2013).
[22] D. Abriola, M. Bostan, S. Erturk, M. Fadil, M. Galan, S. Juutinen, T. Kibédi, F. Kondev, A. Luca, A. Negret, N. Nica, B. Pfeiffer, B. Singh, A. Sonzogni, J. Timar, J. Tuli, T. Venkova, and K. Zuber, Nucl. Data Sheets **110**, 2815 (2009).
[23] G. Jakob, N. Benczer-Koller, J. Holden, G. Kumbartzki, T. J. Mertzimekis, K.-H. Speidel, R. Ernst, P. Maier-Komor, C. W. Beausang, and R. Krücken, Phys. Lett. B **494**, 187 (2000).
[24] P. F. Mantica, A. E. Stuchbery, D. E. Groh, J. I. Prisciandaro, and M. P. Robinson, Phys. Rev. C **63**, 034312 (2001).
[25] P. von Neumann-Cosel, A. Poves, J. Retamosa, and A. Richter, Phys. Lett. B **443**, 1 (1998).
[26] R. Machleidt, Phys. Rev. C **63**, 024001 (2001).
[27] M. Hjorth-Jensen, T. T. S. Kuo, and E. Osnes, Phys. Rep. **261**, 125 (1995).
[28] W. Urban, K. Sieja, G. S. Simpson, T. Soldner, T. Rzaca-Urban, A. Złomaniec, I. Tsekhanovich, J. A. Dare, A. G. Smith, J. L. Durell, J. F. Smith, R. Orlandi, A. Scherillo, I. Ahmad, J. P. Greene, J. Jolie, and A. Linneman, Phys. Rev. C **85**, 014329 (2012).
[29] W. Urban, K. Sieja, G. S. Simpson, H. Faust, T. Rzaca-Urban, A. Złomaniec, M. Łukasiewicz, A. G. Smith, J. L. Durell, J. F. Smith, B. J. Varley, F. Nowacki, and I. Ahmad, Phys. Rev. C **79**, 044304 (2009).
[30] K. Sieja, T. R. Rodriguez, K. Kolos, and D. Verney, Phys. Rev. C **88**, 034327 (2013).
[31] T. Rzaca-Urban, K. Sieja, W. Urban, F. Nowacki, J. L. Durell, A. G. Smith, and I. Ahmad, Phys. Rev. C **79**, 024319 (2009).
[32] E. Caurier, G. Martinez-Pinedo, F. Nowacki, A. Poves, and A. P. Zuker, Rev. Mod. Phys. **77**, 427 (2005).
[33] B. A. Brown and B. H. Wildenthal, Annu. Rev. Nucl. Part. Sci **38**, 29 (1988).